# Isolated Triggered Tremor Spots in South America and Implications for Global Tremor Activity

by Kevin Chao, Zhigang Peng, William B. Frank, Germán A. Prieto, and Kazushige Obara

## ABSTRACT

We report new observations of triggered tectonic tremor in three regions in South America along the plate boundary between the Nazca and South America plates: southern Chile, Ecuador, and central Colombia. In these regions, tremor was observed during the passage of large-amplitude surface waves of recent large earthquakes, which occurred in South America and around the world. In southern Chile, triggered tremor was observed around an ambient tremor active zone in the Chile triple junction region. In Ecuador and central Colombia, only one seismic station in each region recorded triggered tremor. With a single-station approach, we are able to estimate potential tremor sources in these regions. Triggered tremor in Ecuador is likely associated with an inland fault near the volcanic region. In central Colombia, triggered tremor may be associated with the Romeral fault system rather than the subduction zone interface. In addition, we summarize global observations of tremor-triggering stress and background ambient tremor activity in 24 tremor-active regions. Based on the global summary of triggered and ambient tremor activity, the relative lack of triggered tremor in central and northern Chile and Peru is consistent with the lack of background tremor activity in these regions, suggesting tectonic tremor occurs only in isolated regions along major faults.

*Supplemental Content:* Figure showing example seismograms of nontriggered tremor in Peru and figure demonstrating a comparison between single-station and multiple-station methods.

## INTRODUCTION

Deep tectonic tremor, which occurs below seismogenic zones (Gao and Wang, 2017), is often associated with slow-slip events (SSEs; Beroza and Ide, 2011). Because of their extreme sensitivity to stress, tremor and SSEs could provide important information for monitoring stress variations in regions of large earthquakes in seismogenic zones (Kato *et al.*, 2012; Kato and Nakagawa, 2014; Ruiz *et al.*, 2014; Obara and Kato, 2016; Uchida *et al.*, 2016). Although SSEs must exceed a certain size (e.g., at least with a moment magnitude of ~5) to be recorded by current geodetic instrumentation, observations of tectonic tremor are also important for detecting small-magnitude SSEs (Frank *et al.*, 2015; Frank, 2016; Rousset *et al.*, 2019).

With ample observations of tectonic tremor along major plate boundaries (Peng and Gomberg, 2010; Beroza and Ide, 2011; Obara and Kato, 2016; and references therein) and inland fault systems (Aiken *et al.*, 2015; Chao and Obara, 2016), studies suggested this seismic phenomenon might occur in most major fault systems (Peng and Gomberg, 2010; Beroza and Ide, 2011). Several studies, however, suggested tectonic tremor cannot be identified in many active faults or regions where tremor is expected (Suzuki and Yamashita, 2009; Gomberg *et al.*, 2012; Yang and Peng, 2013; Bockholt *et al.*, 2014; Pfohl *et al.*, 2015; Bansal *et al.*, 2016; Inbal *et al.*, 2018).

The western coast of South America is a major convergent plate boundary, which separates the Nazca and South America plates to the north and the Antarctic and South America plates in southern Chile (Fig. 1). Compared to other tectonic regions with abundant observations of tectonic tremor, such as that around the Pacific Rim (Peng and Gomberg, 2010; Chao *et al.*, 2013), only near the triple junction area in Chile has tremor been observed (Ide, 2012; Gallego *et al.*, 2013; Saez *et al.*, 2019). A recent study, however, reported SSEs near the shallow subduction interface in Ecuador (Vallée *et al.*, 2013). In central Chile, multiple episodic SSEs may have preceded the 2014 $M_w$ 8.2 Iquique earthquake (Kato and Nakagawa, 2014), but Bedford *et al.* (2015) also suggested the geodetic signals before the Iquique mainshock require no additional SSEs to explain their occurrence. Nevertheless, tectonic tremor has not been observed in these regions, and it is still not clear whether this finding reflects a genuine lack of tremor in these regions or an absence of continuous high-quality and high-density seismic recordings.

Many studies have shown tremor can be triggered instantaneously during large-amplitude surface waves of distant earthquakes (e.g., Peng and Gomberg, 2010). Because triggered

 doi: 10.1785/0220190009

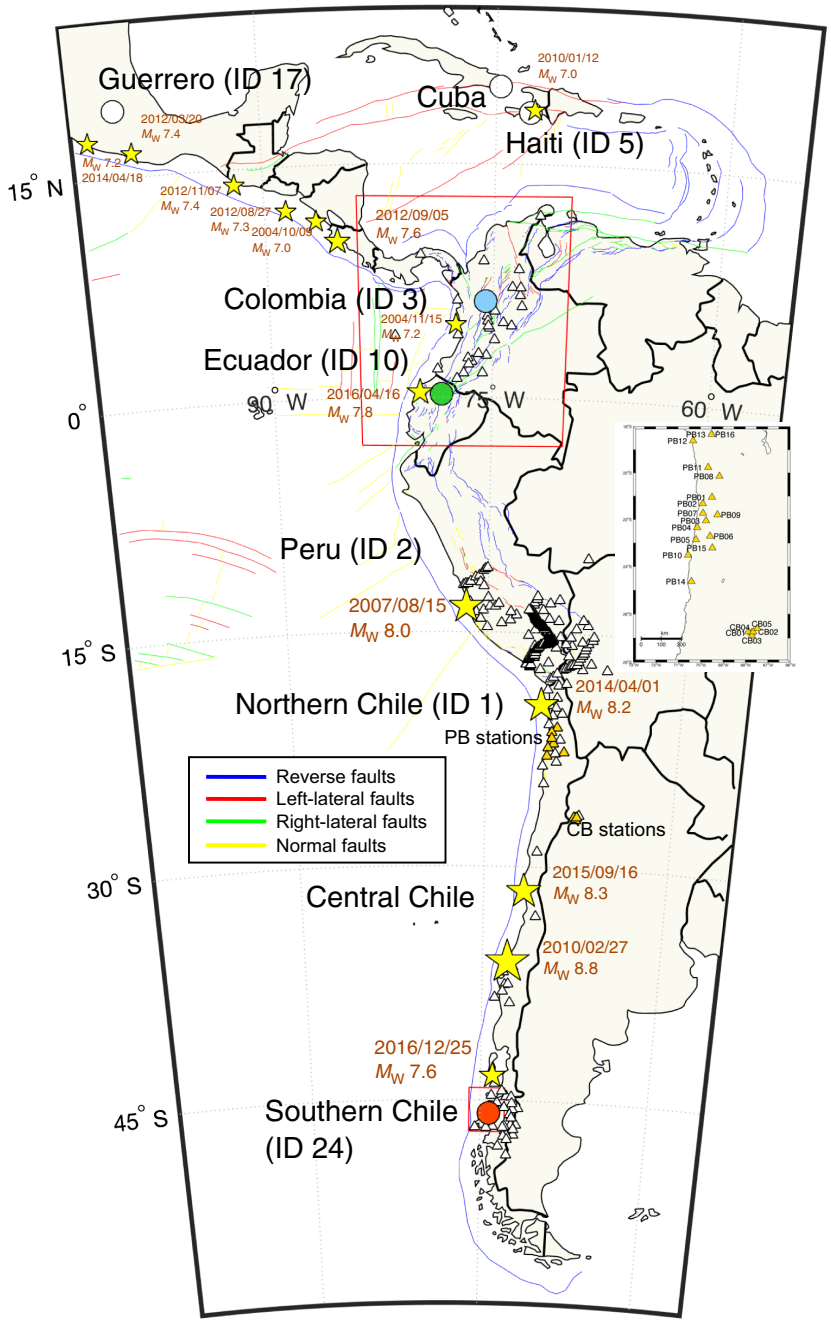


▲ **Figure 1.** Map of the study region in South America. Triangles represent the seismic stations used in this study. Colored circles indicate the newly observed triggered tremor sources in southern Chile, Ecuador, and central Colombia. Open circles represent triggered tremor observed by previous studies in Guerrero, Mexico (Zigone *et al.*, 2012), Cuba (Peng *et al.*, 2013), and Haiti (Aiken *et al.*, 2016). The color version of this figure is available only in the electronic edition.

tremor mostly occurs in regions with ambient tremor (e.g., Chao *et al.*, 2013), they are considered the same physical processes, except triggered tremor is driven by the stress perturbation of teleseismic surface waves (Gomberg, 2010), whereas ambient tremor (i.e., tremor does not occur during surface waves) is likely driven by normal SSEs. Hence, a systematic search of triggered tremor could provide a useful tool for mapping tremorgenic regions. In addition, triggered tremor has higher amplitude than ambient tremor (Rubinstein *et al.*, 2007; Peng *et al.*, 2008) and occurs only during the passing surface waves of large teleseismic earthquakes (e.g., $M_w \geq 7.5$). Hence, identifying them by examining modulating high-frequency nonearthquake signals during surface waves is more efficient than scanning years of continuous waveforms for ambient tremor.

Previous studies have shown triggered tremor can be identified by single-station observation (Fuchs *et al.*, 2014; Bansal *et al.*, 2016; Chao and Obara, 2016; Peng *et al.*, 2013, 2018). However, using a one-station recording to locate a tremor source region, particularly in regions with multiple active fault systems (Fuchs *et al.*, 2014; Chao and Obara, 2016), is virtually impossible. Thus, developing an approach to locating triggered tremor from a single station could expand our knowledge of the tremor-generation environment.

In this study, we examine triggered tremor along the western coast of South America in Chile, Peru, Ecuador, and Colombia. In addition, we introduce a simple method for locating a tremor source from the *S*–*P* time of a single-station recording. We also compare observations of triggered and ambient tremor around the world to explore possible reasons for the lack of observations of tremor in other regions.

## ANALYTICAL PROCEDURES

### Identification of Triggered Tremor

In each region along the western coast of South America (Figs. 1 and 2), we examined all available seismic data for evidence of triggered tremor during the passing surface waves of teleseismic earthquakes. We selected eligible distant mainshocks from the 2001–2016 Advanced National Seismic System (ANSS) earthquake catalog with the following general criteria: $M_w \geq 7.5$, depth ≤ 100 km, epicenter distance ≥ 1000 km, and theoretical dynamic stress ≥ 5.0 kPa from each region (Chao, Peng, Wu, *et al.*, 2012; Aiken *et al.*, 2013; Chao *et al.*, 2013). If any triggered tremor was observed in each region, we examined additional events with smaller calculated dynamic stresses (i.e., greater than 2.0 kPa) based on the epicentral distance and mainshock magnitude (van der Elst and Brodsky, 2010). Because the availability of seismic data differs from region to region, the selected distant earthquakes vary slightly, depending on each area (Table 1).

We began our study by filtering seismograms with a 2–8 Hz band-pass filter or a 5 Hz high-pass filter (applied only if the epicenter distance of a triggering earthquake was less than

**Table 1**
**List of Target Triggering Earthquakes Examined in This Study in Southern Chile, Ecuador, and Central Colombia**

| Date (yyyy/mm/dd) | Time (hh:mm:ss.ss) | Longitude (°) | Latitude (°) | Depth (km) | $M_w$ | Distance (km) | kPa | Quality |
|---|---|---|---|---|---|---|---|---|
| Southern Chile* | | | | | | | | |
| 2004/12/23 | 14:59:04.41 | 161.3450 | −49.3120 | 10.0 | 8.1 | 8223.6 | 3.1 | 0 |
| 2004/12/26 | 00:58:53.45 | 95.9820 | 3.2950 | 30.0 | 9.0 | 15232.4 | 8.9 | 1 |
| 2005/03/28 | 16:09:36.53 | 97.1080 | 2.0850 | 30.0 | 8.6 | 15121.7 | 3.6 | 1 |
| 2006/05/03 | 15:26:40.29 | −174.1230 | −20.1870 | 55.0 | 8.0 | 9191.6 | 2.1 | 1 |
| Ecuador† | | | | | | | | |
| 2001/01/13 | 17:33:32.38 | −88.6600 | 13.0490 | 60.0 | 7.7 | 1808.1 | 15.4 | 0 |
| 2001/06/23 | 20:33:14.13 | −73.6410 | −16.2650 | 33.0 | 8.4 | 1898.1 | 71.1 | n/a |
| 2001/07/07 | 09:38:43.52 | −72.0770 | −17.5430 | 33.0 | 7.6 | 2084.8 | 9.6 | n/a |
| 2003/01/22 | 02:06:34.61 | −104.1040 | 18.7700 | 24.0 | 7.6 | 3468.8 | 4.1 | n/a |
| 2003/09/25 | 19:50:06.36 | 143.9100 | 41.8150 | 27.0 | 8.3 | 13714.2 | 2.1 | n/a |
| 2004/12/26 | 00:58:53.45 | 95.9820 | 3.2950 | 30.0 | 9.1 | 19282.7 | 7.6 | 1 |
| 2005/03/28 | 16:09:36.53 | 97.1080 | 2.0850 | 30.0 | 8.6 | 19457.8 | 2.4 | 0 |
| 2006/11/15 | 11:14:13.57 | 153.2660 | 46.5920 | 10.0 | 8.3 | 12798.4 | 2.4 | 0 |
| 2007/08/15 | 23:40:57.89 | −76.6030 | −13.3860 | 39.0 | 8.0 | 1518.7 | 41.0 | 1 |
| 2007/11/14 | 15:40:50.53 | −69.8900 | −22.2470 | 40.0 | 7.7 | 2652.5 | 8.1 | 0 |
| 2009/09/29 | 17:48:10.99 | −172.0950 | −15.4890 | 18.0 | 8.1 | 10404.7 | 2.1 | 0 |
| 2010/02/27 | 06:34:11.53 | −72.8980 | −36.1220 | 22.9 | 8.8 | 4063.1 | 50.5 | 1 |
| 2011/03/11 | 05:46:24.12 | 142.3730 | 38.2970 | 29.0 | 9.1 | 14050.0 | 12.8 | 0 |
| 2012/04/11 | 08:38:36.72 | 93.0630 | 2.3270 | 20.0 | 8.6 | 19029.2 | 2.5 | 0 |
| 2012/09/05 | 14:42:07.80 | −85.3150 | 10.0850 | 35.0 | 7.6 | 1326.5 | 20.4 | 0 |
| 2014/04/01 | 23:46:47.26 | −70.7691 | −19.6097 | 25.0 | 8.2 | 2347.6 | 31.5 | n/a |
| 2014/04/03 | 02:43:13.11 | −70.4931 | −20.5709 | 22.4 | 7.7 | 2457.1 | 9.2 | n/a |
| 2015/09/16 | 22:54:32.86 | −71.6744 | −31.5729 | 22.4 | 8.3 | 3589.5 | 19.6 | 0 |
| 2016/12/25 | 14:22:27.01 | −73.9413 | −43.4064 | 38.0 | 7.6 | 4852.1 | 2.4 | n/a |
| 2017/09/08 | 04:49:19.18 | −93.8993 | 15.0222 | 47.4 | 8.2 | 2355.9 | 31.3 | 0 |
| 2018/01/10 | 02:51:33.29 | −83.5200 | 17.4825 | 19.0 | 7.5 | 1984.5 | 8.3 | 0 |
| Central Colombia‡ | | | | | | | | |
| 2010/02/27 | 06:34:11.53 | −72.8980 | −36.1220 | 22.9 | 8.8 | 4687.9 | 39.8 | 1 |
| 2011/03/11 | 05:46:24.12 | 142.3730 | 38.2970 | 29.0 | 9.1 | 13726.1 | 13.3 | 0 |
| 2012/04/11 | 08:38:36.72 | 93.0630 | 2.3270 | 20.0 | 8.6 | 18436.4 | 2.6 | n/a |
| 2012/09/05 | 14:42:07.80 | −85.3150 | 10.0850 | 35.0 | 7.6 | 1159.8 | 25.5 | 0 |

kPa, kilopascal; $M_w$, moment magnitude; PGV, stress (kPa) converted from peak ground velocity.

*Theoretical dynamic stress computed at station YJ.HUM01 (longitude −73.9591°, latitude −45.5578°) for distance > 1000 (km); $M_w \geq 7.5$; PGV ≥ 2.0 (kPa); years: 11 December 2004–31 December 2006. Quality, 0 denotes nontriggered and 1 denotes triggered tremor.

†Theoretical dynamic stress computed at station IU.OTAV (longitude −78.4508°, latitude 0.2376°) for distance > 1000 (km); $M_w \geq 7.5$; PGV ≥ 2.0 (kPa); years: 1 January 2001–1 October 2018. Quality, 0 denotes nontriggered and 1 denotes triggered tremor; n/a, no data.

‡Theoretical dynamic stress computed at station CM.HEL (longitude −75.5288°, latitude 6.1908°) for distance > 1000 (km); $M_w \geq 7.5$; PGV ≥ 2.0 (kPa); years: 1 January 2010–31 December 2017. Quality, 0 denotes nontriggered and 1 denotes triggered tremor; n/a, no data.

§Theoretical dynamic stress computed at station CX.PB04 (longitude −70.1492°, latitude −22.3337°) for distance > 1000 (km); $M_w \geq 7.5$; PGV ≥ 5.0 (kPa); years: 1 January 2004–31 December 2017. Quality, 0 denotes nontriggered and 2 denotes triggered earthquake.

‖Theoretical dynamic stress computed at station II.NNA (longitude −76.8422°, latitude −11.9875°) for distance > 800 (km); $M_w \geq 7.5$; PGV ≥ 5.0 (kPa); years: 1 January 2004–1 October 2018. Quality, 0 denotes nontriggered.

(Continued next page.)

**Table 1 (continued)**
**List of Target Triggering Earthquakes Examined in This Study in Southern Chile, Ecuador, and Central Colombia**

| Date (yyyy/mm/dd) | Time (hh:mm:ss.ss) | Longitude (°) | Latitude (°) | Depth (km) | $M_w$ | Distance (km) | kPa | Quality |
|---|---|---|---|---|---|---|---|---|
| 2014/04/01 | 23:46:47.26 | −70.7691 | −19.6097 | 25.0 | 8.2 | 2897.9 | 22.2 | 0 |
| 2014/04/03 | 02:43:13.11 | −70.4931 | −20.5709 | 22.4 | 7.7 | 3007.8 | 6.6 | 0 |
| 2015/09/16 | 22:54:32.86 | −71.6744 | −31.5729 | 22.4 | 8.3 | 4195.3 | 15.1 | 0 |
| 2017/09/08 | 04:49:19.18 | −93.8993 | 15.0222 | 47.4 | 8.2 | 2230.5 | 34.3 | 0 |
| Northern Chile[§] | | | | | | | | |
| 2004/12/26 | 00:58:53.45 | 95.9820 | 3.2950 | 30.0 | 9.1 | 17432.3 | 9.0 | 2 |
| 2007/08/15 | 23:40:57.89 | −76.6030 | −13.3860 | 39.0 | 8.0 | 1202.0 | 60.4 | 2 |
| 2010/02/27 | 06:34:11.53 | −72.8980 | −36.1220 | 22.9 | 8.8 | 1550.7 | 249.6 | 2 |
| 2011/03/11 | 05:46:24.12 | 142.3730 | 38.2970 | 29.0 | 9.1 | 16448.9 | 9.9 | 2 |
| 2015/09/16 | 22:54:32.86 | −71.6744 | −31.5729 | 22.4 | 8.3 | 1034.3 | 154.6 | 2 |
| 2016/04/16 | 23:58:36.98 | −79.9218 | 0.3819 | 20.6 | 7.8 | 2724.8 | 9.8 | 2 |
| 2016/12/25 | 14:22:27.01 | −73.9413 | −43.4064 | 38.0 | 7.6 | 2362.8 | 7.8 | 2 |
| 2017/09/08 | 04:49:19.18 | −93.8993 | 15.0222 | 47.4 | 8.2 | 4872.0 | 9.4 | 2 |
| Peru[‖] | | | | | | | | |
| 2004/12/26 | 00:58:53.45 | 95.9820 | 3.2950 | 30.0 | 9.1 | 18770.7 | 7.9 | 0 |
| 2007/11/14 | 15:40:50.53 | −69.8900 | −22.2470 | 40.0 | 7.7 | 1353.3 | 24.9 | 0 |
| 2010/02/27 | 06:34:11.53 | −72.8980 | −36.1220 | 22.9 | 8.8 | 2701.0 | 99.4 | 0 |
| 2011/03/11 | 05:46:24.12 | 142.3730 | 38.2970 | 29.0 | 9.1 | 15163.4 | 11.3 | 0 |
| 2012/09/05 | 14:42:07.80 | −85.3150 | 10.0850 | 35.0 | 7.6 | 2611.8 | 6.6 | 0 |
| 2014/04/01 | 23:46:47.26 | −70.7691 | −19.6097 | 25.0 | 8.2 | 1063.9 | 117.2 | 0 |
| 2014/04/03 | 02:43:13.11 | −70.4931 | −20.5709 | 22.4 | 7.7 | 1165.9 | 31.8 | 0 |
| 2015/09/16 | 22:54:32.86 | −71.6744 | −31.5729 | 22.4 | 8.3 | 2231.2 | 43.2 | 0 |
| 2016/04/16 | 23:58:36.98 | −79.9218 | 0.3819 | 20.6 | 7.8 | 1408.1 | 29.3 | 0 |
| 2017/09/08 | 04:49:19.18 | −93.8993 | 15.0222 | 47.4 | 8.2 | 3525.9 | 16.0 | 0 |

kPa, kilopascal; $M_w$, moment magnitude; PGV, stress (kPa) converted from peak ground velocity.
*Theoretical dynamic stress computed at station YJ.HUM01 (longitude −73.9591°, latitude −45.5578°) for distance > 1000 (km); $M_w \geq 7.5$; PGV ≥ 2.0 (kPa); years: 11 December 2004–31 December 2006. Quality, 0 denotes nontriggered and 1 denotes triggered tremor.
[†]Theoretical dynamic stress computed at station IU.OTAV (longitude −78.4508°, latitude 0.2376°) for distance > 1000 (km); $M_w \geq 7.5$; PGV ≥ 2.0 (kPa); years: 1 January 2001–1 October 2018. Quality, 0 denotes nontriggered and 1 denotes triggered tremor; n/a, no data.
[‡]Theoretical dynamic stress computed at station CM.HEL (longitude −75.5288°, latitude 6.1908°) for distance > 1000 (km); $M_w \geq 7.5$; PGV ≥ 2.0 (kPa); years: 1 January 2010–31 December 2017. Quality, 0 denotes nontriggered and 1 denotes triggered tremor; n/a, no data.
[§]Theoretical dynamic stress computed at station CX.PB04 (longitude −70.1492°, latitude −22.3337°) for distance > 1000 (km); $M_w \geq 7.5$; PGV ≥ 5.0 (kPa); years: 1 January 2004–31 December 2017. Quality, 0 denotes nontriggered and 2 denotes triggered earthquake.
[‖]Theoretical dynamic stress computed at station II.NNA (longitude −76.8422°, latitude −11.9875°) for distance > 800 (km); $M_w \geq 7.5$; PGV ≥ 5.0 (kPa); years: 1 January 2004–1 October 2018. Quality, 0 denotes nontriggered.

1500 km) (Guilhem *et al.*, 2010) and then compared them with the long-period Love and Rayleigh waves of distant earthquakes. We identified triggered tremor as coherent high-frequency, non-impulsive signals recorded by surrounding stations during the passing surface waves of teleseismic earthquakes (Chao, Peng, Wu, *et al.*, 2012; Chao *et al.*, 2013) through visual identification with the Seismic Analysis Code (Helffrich *et al.*, 2013) and CrazyTremor (Chao and Yu, 2018) software. If a single station recorded a potentially triggered tremor signal, we adopted the following two measurements to further confirm the reliability of tremor observation: (1) the cross-correlation value and (2) the signal-to-noise ratio (SNR). The first criterion requires triggered tremor be modulated by surface waves (Fig. 3). We computed the correlation coefficient (CC) between the broadband surface waves (100–1 s) and high-frequency envelope functions (2–8 or >5 Hz), smoothed with a half-length of 100 data points. The CC value had to be larger than 0.2 (Chao, Peng, Wu, *et al.*, 2012). According to the second criterion, the SNR

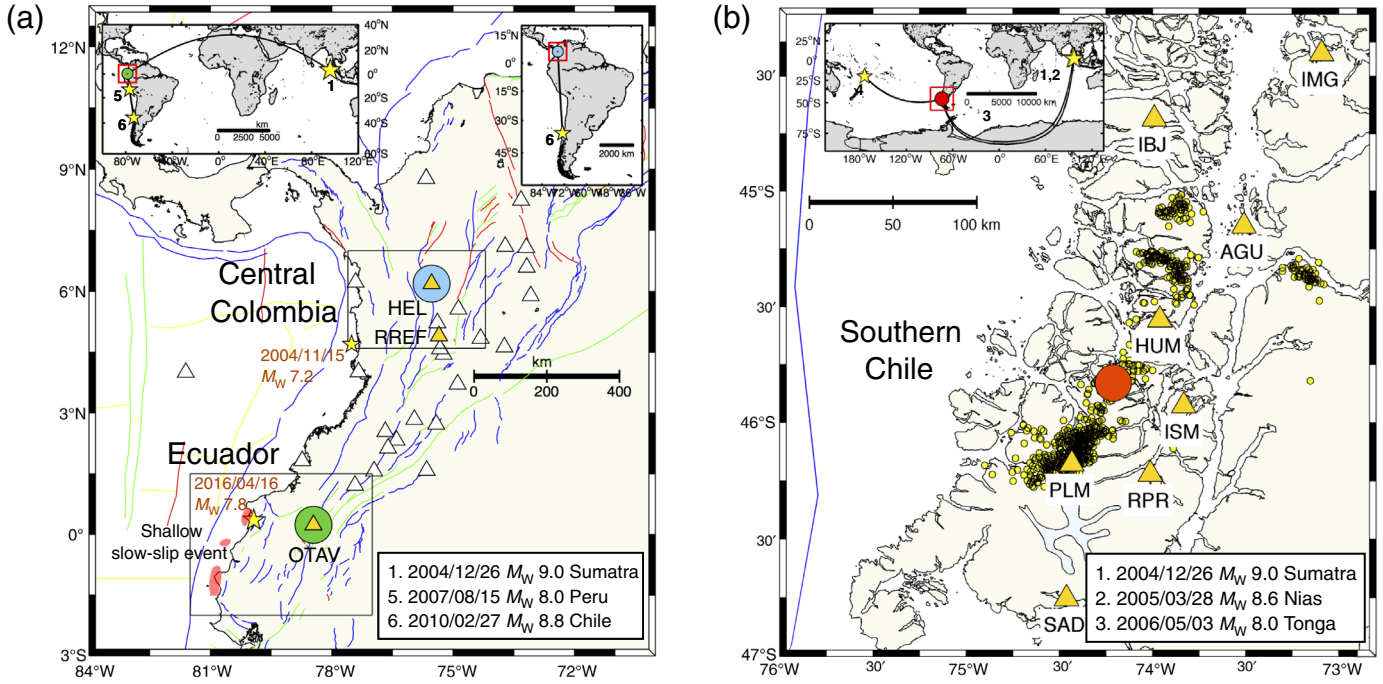


▲ **Figure 2.** (a) Triggered tremor sources observed by the OTAV station in Ecuador (green circle) and the HEL station in central Colombia (blue circle). Pink shaded areas in Ecuador indicate sources of slow-slip events (SSEs; Vallée *et al.*, 2013). (b) Triggered tremor (red circle) in southern Chile. Small yellow circles mark the ambient tremor locations from 1 January 2005 to 28 February 2007, observed by the clustered method by Idehara *et al.* (2014). (Insets) Triggering teleseismic earthquakes in each region. The color version of this figure is available only in the electronic edition.

of the tremor signal to the background noise had to exceed 1.5 (Chao, Peng, Fabian, and Ojha, 2012). Finally, we ensured the same station recorded triggered tremor from different teleseismic earthquakes, if applicable (Table 1).

### Locations of Triggered Tremor

We used two methods to locate tremor sources, depending on whether they were recorded by a single station or multiple stations. For tremor signals recorded by several stations, we applied the standard envelope cross-correlation method to perform a grid search for the location (e.g., Wech and Creager, 2008). By computing the root mean square (rms) value for each grid point from the observational and theoretical travel-time difference for all station pairs at each grid point, the tremor source was the point with the minimum rms value (Chao *et al.*, 2013; Chao and Obara, 2016). For tremor recorded by one station, we applied a single-station approach to estimate the potential source. The purpose of this approach, based primarily on filtering triggered tremor with several frequency bands, was to identify potential *S*–*P* times. The detailed steps of the analysis appear in Appendix.

## OBSERVATIONS OF TRIGGERED TREMOR IN SOUTH AMERICA

### Southern Chile

We collected seismic data in southern Chile from a temporary array consisting of 26 stations (the Chile ridge subduction seismic network, see Data and Resources) operating from December 2004 to December 2006. Among the four selected distant earthquakes (Table 1), we identified three events that triggered clear tremor events in this region (26 December 2004 $M_w$ 9.0 Sumatra, 28 March 2005 $M_w$ 8.6 Nias, and the 3 May 2006 $M_w$ 8.0 Tonga earthquakes). For the 2004 Sumatra and 2005 Nias events, tremor first occurred during the arrival of body waves and remained active with later passing surface waves with a total duration of ~3000 and 1500 s, respectively (Fig. 3a,b). We measured the total duration as the time span between the start and the end of triggered tremor, even though there were obvious time gaps when tremor was impeded by the passing surface waves. In contrast, the total duration of the tremor triggered by the 2006 Tonga event (Fig. 3c) was only ~700 s during the passing of Love and Rayleigh waves. The much longer tremor durations of these 2004 Sumatra and 2005 Nias events were simply due to the longer surface-wave durations associated with the longer propagation distances of these two mainshocks.

Triggered tremor was roughly located around the ambient tremor-active region (Fig. 2b) (Ide, 2012; Gallego *et al.*, 2013; Idehara *et al.*, 2014), the probable location of multiple triggered tremor sources (Fig. 3a,b). Because of a lack of sufficient station coverage and the (inadequate?) resolution of the envelope cross-correlation method, however, we were unable to obtain a well-constrained tremor depth.

### Ecuador

Ecuador has two seismic stations, OTAV and PAYG in the Incorporated Research Institutions for Seismology (IRIS)

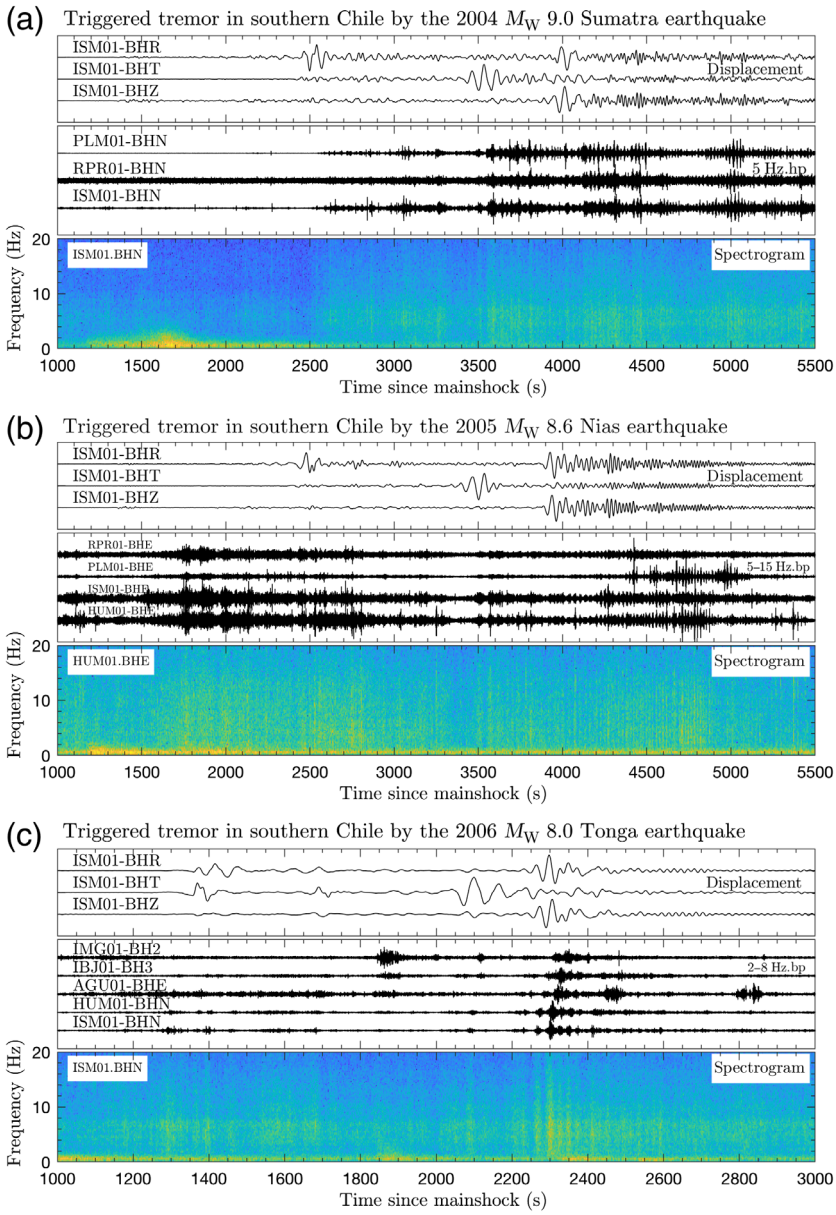


▲ **Figure 3.** Seismograms of newly observed triggered tremor in southern Chile following (a) the 2004 $M_w$ 9.0 Sumatra, (b) the 2005 $M_w$ 8.6 Nias, and (c) the 2006 $M_w$ 8.0 Tonga earthquakes. The color version of this figure is available only in the electronic edition.

Global Seismograph Network (GSN). Because GSN has been in operation for a long time, we acquired information on 21 teleseismic earthquakes for further analysis. Among these events, we observed triggered tremor following the 26 December 2004 $M_w$ 9.0 Sumatra, the 15 August 2007 $M_w$ 8.0 Peru, and the 27 February 2010 $M_w$ 8.8 Chile earthquakes only at station OTAV (Fig. 4). A previous study also observed triggered earthquakes at station OTAV following the 2004 $M_w$ 9.0 Sumatra (Velasco *et al.*, 2008) and 2011 $M_w$ 9.0 Tohoku-Oki earthquake (Gonzalez-Huizar *et al.*, 2012). Another nearby station, GCAL, about 157 km northeast of OTAV (Fig. 5e), did not record any triggered tremor signals. Using the single-station algorithm in the Appendix, we observed an *S*–*P* time delay of 3.3 s in tremor lasting between 1140 and 1250 s following the 2010 Chile mainshock (Fig. 5d). This time delay corresponds to a hypocenter distance of about 29 km from the OTAV station. Because station OTAV is ~180 km to the east of the SSE active region along the Ecuadorian subduction zone (Vallée *et al.*, 2013; Rolandone *et al.*, 2018), and the subduction interface is at least 80 km below OTAV, we infer the tremor source was not associated with the subduction interface, but more likely with inland faults (Figs. 2a and 4e).

## Central Colombia

In Colombia, we examined 32 seismic stations operated by the Servicio Geologico Colombiano (SGC) and other regional seismic networks from January 2010 to November 2016 (Fig. 2a). Among eight teleseismic earthquakes, the 2010 Chile earthquake triggered clear tremor at the HEL station, located in central Colombia. As shown in Figure 6, triggered tremor occurred mainly during the passing Rayleigh waves. The average *S*–*P* time was 3.1 s, which corresponds to a hypocenter distance of about 27 km to the HEL station (Fig. 5f,g). One station, RREF, located about 144 km south of the HEL station, also recorded plausible high-frequency signals during the first few cycles of the Rayleigh waves (Fig. 6b). The triggered signals at station RREF, however, had shorter durations and a sharper onset. They were therefore more likely to be triggered earthquakes rather than triggered tremor with longer duration and a more gradual onset (e.g., Aiken *et al.*, 2015).

Compared to the 2010 Chile earthquake, the 2011 $M_w$ 9.0 Tohoku-Oki earthquake triggered tremor in many parts of the world (Chao *et al.*, 2013), but not in central Colombia or Ecuador, likely the result of the dynamic stress it had generated (13.3 kPa, Table 1), which was relatively less than that generated by the surface waves of the Chile earthquake (39.8 kPa).

Because triggered and ambient tremors generally have lower SNRs than typical earthquakes, it can be recorded only by seismic stations within ~40–60 km of the tremor source (Chao *et al.*, 2017). If we assume tremor originated in a very localized fault near the HEL station, its source could have been associated with several tectonic environments (Fuchs *et al.*, 2014). One is the strike-slip Romeral fault system (Ego *et al.*, 1995; Dimate *et al.*, 2003; Chicangana, 2005), which suggests the tremor near the HEL station, was similar to that in Parkfield in central California (Shelly and Hardebeck, 2010) and an inland fault tremor in Japan (Chao and Obara, 2016), was located at a relatively shallow depth (i.e., between 15 and 25 km). Another possible

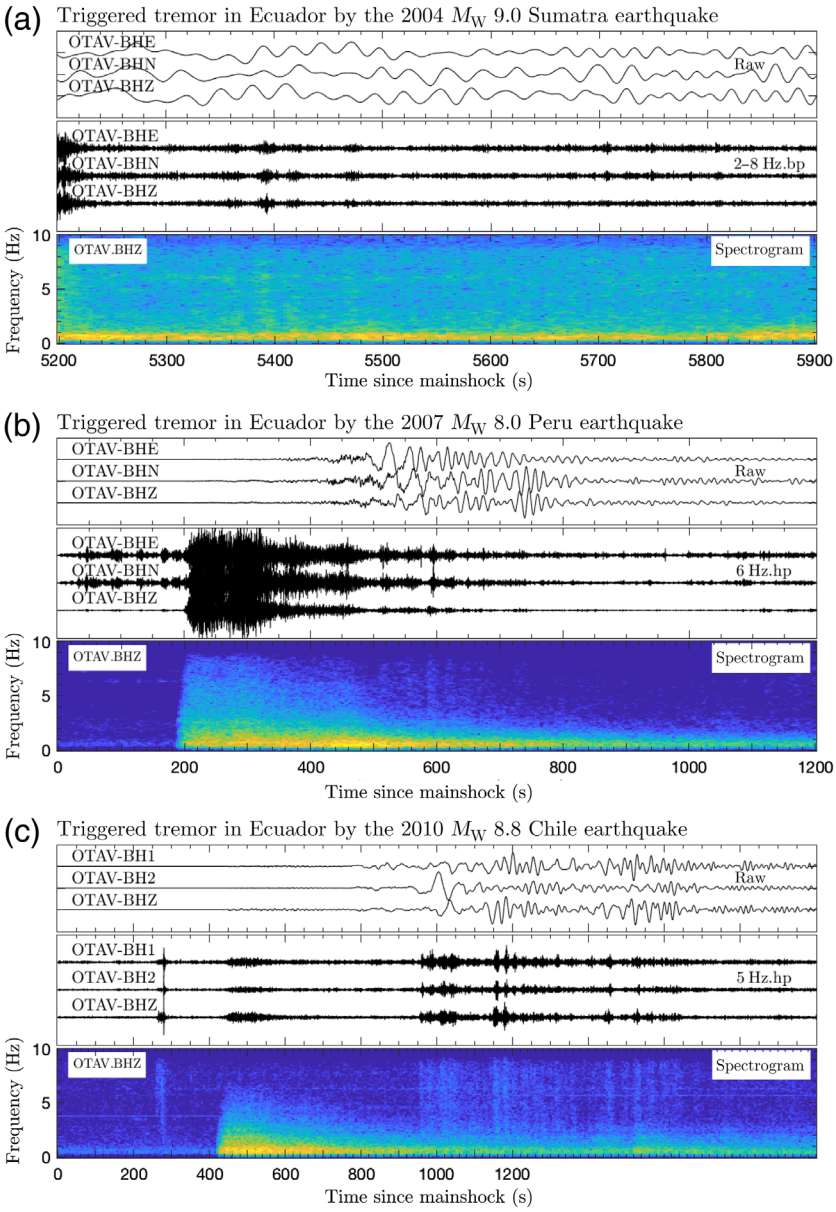


▲ **Figure 4.** Newly observed triggered tremor in Ecuador recorded at the OTAV station during the passing surface waves of (a) the 2004 $M_w$ 9.0 Sumatra, (b) the 2007 $M_w$ 8.0 Peru, and (c) the 2010 $M_w$ 8.8 Chile earthquakes. The color version of this figure is available only in the electronic edition.

tectonic environment is the subduction interface of the Nazca plate to the west (Chiarabba *et al.*, 2016; Syracuse *et al.*, 2016; Wagner *et al.*, 2017) or the Caribbean plate to the north (Bezada *et al.*, 2010; Bernal-Olaya *et al.*, 2015). Because the HEL station, however, is at least a few hundred kilometers from the trenches on both sides, the observed triggered tremor is not likely associated with these subduction interfaces, but instead with the nearby Romeral strike-slip fault system.

## Central and Northern Chile and Peru

Chile has permanent stations from the Chilean National Seismic Network and the plate boundary seismic network (see Data and Resources for details). In addition, several temporal seismic arrays were deployed in central and northern Chile after the 2010 $M_w$ 8.8 Chile earthquake. This study examined eligible teleseismic earthquakes between January 2004 and December 2017 with all available open seismic datasets (Table 1). Although we did not observe any potential triggered tremor signals in these regions, we did observe active triggered earthquake activity (i.e., short durations and sudden onsets) at the CB and PB stations during the passing surface waves (Fig. 7). In Peru, GSN station NNA has been in operation since 2004. Although 10 earthquakes generated large dynamic stress (6–120 kPa) capable of dynamically triggering regular earthquakes, we did not identify clear triggered tremor during surface waves (Ⓔ Fig. S1, available in the supplemental content to this article) at station NNA or other temporary stations in southern Peru.

## Global Comparison of Tremor-Triggering Stress

In this section, we compared observations of tremor-triggering stress and background ambient tremor activities in 24 regions (i.e., 19 regions from previous studies and five from this study; Fig. 8) (Kano *et al.*, 2018). The minimum dynamic stresses of Rayleigh waves in each region were either observations from previous papers (i.e., see the caption of Fig. 8) or directly measured from the surface-wave seismograms in this article (Chao *et al.*, 2013; Chao and Obara, 2016). Because these regions include various types of tectonic environments, such as subduction zones and strike-slip faults along major plate boundaries and other inland faulting systems, we separated them into four groups based on background ambient tremor activity and the number of observed tremor-triggering events. Group I includes regions with ambient tremor and at least two tremor-triggering events (e.g., Nankai, Vancouver Island, Parkfield, and Taiwan). Group II contains regions with at least two tremor-triggering events but with questionable (e.g., San Jacinto fault, Hutchison and Ghosh, 2017; Inbal *et al.*, 2018) or no reported (e.g., Queen Charlotte margin, Aiken *et al.*, 2013) ambient tremor events, and inland fault regions in Japan, Chao and Obara, 2016). Groups III and IV are regions with only one (e.g., Haiti, Aiken *et al.*, 2016, and the Calaveras fault in northern California, Chao, Peng, Fabian, and Ojha, 2012) or no tremor-triggering cases. As shown in Figure 8, regions with ambient tremor observations (i.e., group I) tend to have lower triggering thresholds than the remaining groups (either with questionable or no ambient tremor observations).

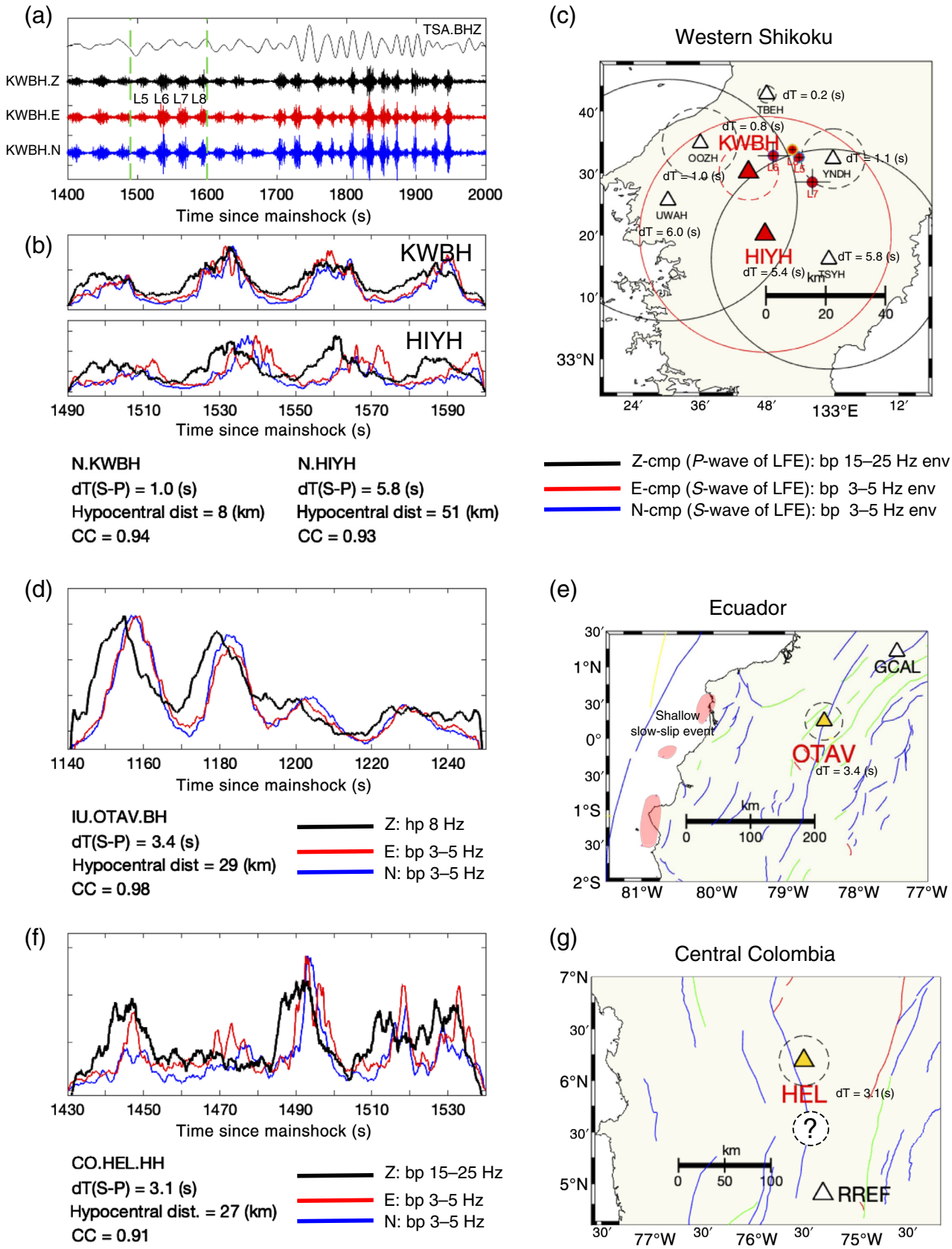


▲ **Figure 5.** Results of the analysis of the single-station approach for testing data in (a–c) western Shikoku in southwestern Japan, (d,e) Ecuador, and (f,g) central Chile. Ⓔ Figure S2 displays the location results of the single-station approach in western Shikoku, Ecuador, and in central Chile. The color version of this figure is available only in the electronic edition.

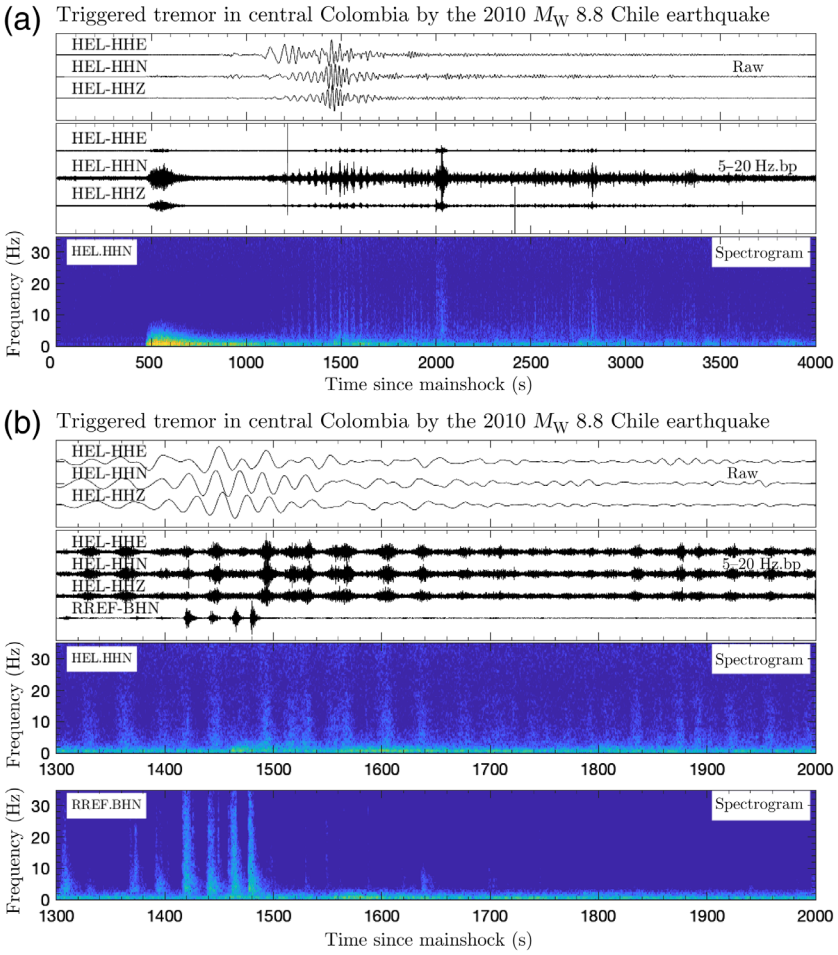


▲ **Figure 6.** (a) Newly observed triggered tremor in central Colombia at the HEL station during the arrival of Rayleigh waves of the 2010 $M_w$ 8.8 Chile earthquake. (b) A zoom-in plot of (a). The color version of this figure is available only in the electronic edition.

## DISCUSSION AND CONCLUSION

This study reported newly observed triggered tremor sources in southern Chile, Ecuador, and central Colombia. Tremor was repeatedly triggered by the surface waves of various teleseismic earthquakes in southern Chile and Ecuador. In southern Chile, triggered tremor was recorded by multiple stations, and the source was located near the triple junction area, where ambient tremor is active (Ide, 2012; Gallego *et al.*, 2013). In northern Chile, we found triggered microearthquakes rather than triggered tremor (Fig. 7). In Ecuador and central Colombia, only a single station in each area recorded triggered tremor. Based on our single-station estimation approach (Fig. 5), we suggest that in central Colombia, triggered tremor originated from the local Romeral strike-slip faulting system (Ego *et al.*, 1995; Dimate *et al.*, 2003; Chicangana, 2005). Similarly in Ecuador, it may have been associated with a local fault rather than the subducting slab near the slow-slip, event-active region (Vallée *et al.*, 2013).

To estimate the potential background tremor activity in Ecuador and central Colombia, we compiled an updated version of tremor-triggering stress around the world (Fig. 8). The observation from this study was generally consistent with the results in Japan (Chao and Obara, 2016), where regions with higher ambient tremor rates are likely to be triggered (i.e., with a lower apparent triggering threshold). From the high tremor-triggering threshold of ~40 kPa we observed in central Colombia, we expect background ambient tremor rate may be low. Hence, denser seismic stations with longer deployed durations are essential for any future search of ambient tremor activity in that region. Ecuador, however, has a lower minimum apparent tremor-triggering threshold of 7.6 kPa (Table 1), suggesting a greater likelihood ambient tremor will occur in the nearby region.

In central and northern Chile and Peru, we did not find clear evidence of triggered tremor. A few stations in northern Chile observed triggered micro-earthquakes during large, distant events. Based on the global comparison between various triggered tremor sources (Fig. 8), we offer several possible explanations for the lack of triggered tremor observations in these regions. One is ambient tremor activity (i.e., not tremor-generic) simply does not occur; another is the lack of high density and continuously recording seismic networks; and the other is no large teleseismic earthquakes generating surface waves with high-dynamic stresses occur. In Peru, we mainly examined seismic data recorded by several temporary deployments of the Program for the Array Seismic Studies of the Continental Lithosphere in 2010–2013. Although several large, distant earthquakes (e.g., the 2011 Tohoku-Oki earthquakes) occurred during this time period, the recordings were relatively short. The 2010 $M_w$ 8.8 Maule mainshock triggered microearthquakes rather than tectonic tremor in northern Chile. Because tremor generally has a lower triggering threshold than micro-earthquakes (Bartlow *et al.*, 2012; Aiken and Peng, 2014), our observations are strongly consistent with the occurrence of no ambient tremor in these regions or the relative difficulty of observing it.

In central Chile (especially around the epicentral regions of the 2010 and 2015 mainshocks), we did not have enough dense seismic stations to rule out the possibility of no triggered (or ambient) tremor in this region. In comparison, we found multiple cases of triggered tremor in the triple junction area of southern Chile, as well as in Ecuador and central Colombia, where the station coverage is reasonable. Ambient tremor has been found in southern Chile (Ide, 2012; Gallego *et al.*, 2013; Saez *et al.*, 2019), but not in the other two regions yet. A common feature of these regions is the incoming plate age is relatively young (e.g., <50 Ma). Previous studies have tried to tie tremor observations with thermal structures of subduction

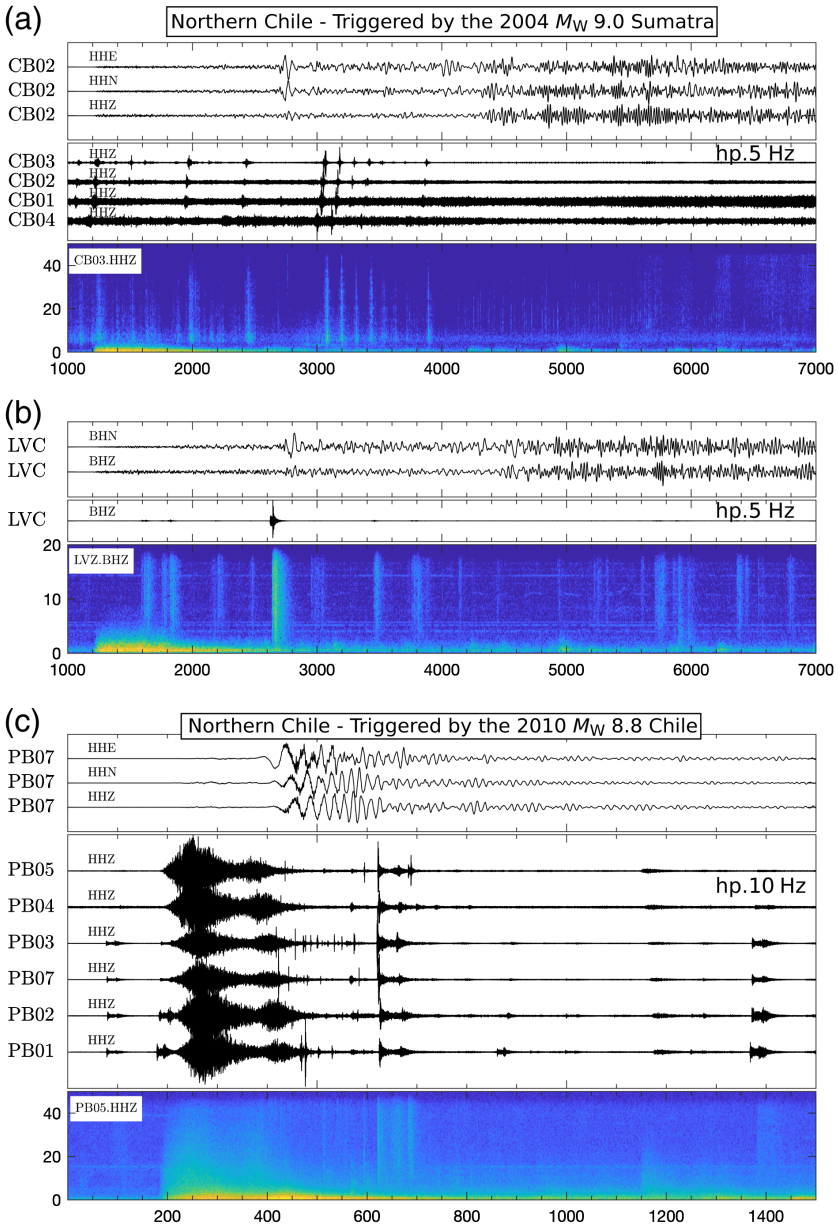


▲ **Figure 7.** Example of triggered earthquakes observed in northern Chile. (a) Triggered earthquakes recorded at the ZQ.CB stations following the 2004 $M_w$ 9.0 Sumatra earthquake. (b) Triggered earthquakes recorded at the GE.LVZ station following the 2004 $M_w$ 9.0 Sumatra earthquake. (c) Triggered earthquakes recorded by the CX.PB stations following the 2010 $M_w$ 8.8 Chile earthquake. The color version of this figure is available only in the electronic edition.

plates (e.g., Obara, 2002). Based on this argument, Beroza and Ide (2011) argued Ecuador and southern Chile would likely be the next places to find tremor. Although the observations of triggered (and ambient) tremor in southern Chile are consistent with our assumption, our observations of triggered tremor in Ecuador and central Colombia do not completely support their argument because the preferred tremor sources are inland faults rather than the subduction interface. Finally, it is worth noting recently tremor (both deep and shallow) has been observed at several places with relatively old incoming plate ages, such as northeastern Japan (e.g., Ito *et al.*, 2015) and the Hikurangi subduction zone in New Zealand (Fry *et al.*, 2011; Ide, 2012; Todd and Schwartz, 2016; Todd *et al.*, 2018).

In conclusion, we observed triggered tremor in the triple junction region in southern Chile, where background ambient tremor is active, and in isolated inland faults in Ecuador and central Colombia. In northern Chile, we observed active triggered earthquakes only during passing surface waves. In central Chile (and northern Peru), it is still unclear if the lack of observations of triggered tremor is merely due to the lack of a tremor source or insufficient seismic networks or triggering earthquakes. Examining additional seismic recordings in these regions during large teleseismic events provides a greater understanding of the geographic distribution of tremor and its underlying physical mechanisms.

## DATA AND RESOURCES

The seismic data in Colombia were provided by the Servicio Geologico Colombiano (SGC). Other data were distributed by the Incorporated Research Institutions for Seismology (IRIS) Data Management Center at http://ds.iris.edu/mda (last accessed October 2018) and the GEOFON Seismological Data Archive operated by the German GeoForschungsZentrum (GFZ) at http://www.webdc.eu/webdc3/ (last accessed October 2018): (1) southern Chile: Chile ridge subduction (network code: YJ, doi: 10.7914/SN/YJ_2004); (2) Ecuador: the Global Seismograph Network (GSN, network code: IU, doi: 10.7914/SN/IU); (3) Colombia: SGC (network codes: CM, permission required at https://www.sgc.gov.co, last accessed September 2018); (4) Peru: the GSN (network code: IU, doi: 10.7914/SN/IU), the study of the Peruvian flat slab (network code: ZD, doi: 10.7914/SN/ZD_2010), the Central Andean uplift and the geodynamics of high topography (network code: ZG, doi: 10.7914/SN/ZG_2010), and the tectonic observatory (network code: TO, doi: 10.7909/C3MW2F2C); (5) Central and northern Chile: Plate boundary observatory network northern Chile (network code: CX, doi: 10.14470/PK615318); Cerro Blanco project central Andes (network code: ZQ); and the Jutland-to-Lower-Saxony (JULS) project (network code: ZW); GEOFON (network code: GE, doi: 10.14470/TR560404). Advanced National Seismic System (ANSS) earthquake catalog can be accessed at http://www.ncedc.org/cnss/catalog-search.html (last accessed November 2016). The ambient tremor catalog in southern Chile can be downloaded at http://www-solid.eps.s.u-tokyo.

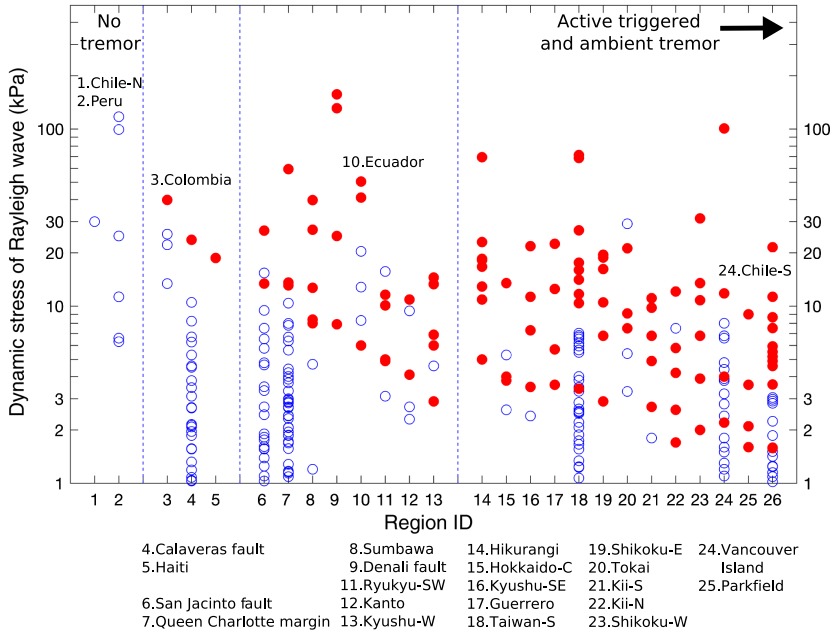


▲ **Figure 8.** Summary of tremor-triggering stress vs. the observations of background ambient tremor in different tectonic regions. The *x* axis is separated into four groups of tectonic regions: active ambient tremor regions (right), active triggered tremor sources with no ambient tremor reports, single observations of triggered tremor, and the regions without any reports of tremor (left). Filled and open circles represent tremor-triggering and nontremor-triggering events, respectively. Region IDs from numbers 1 to 26 correspond to the following regions: (1) northern Chile (this study); (2) Peru (this study); (3) central Colombia (this study); (4) Calaveras fault, northern California (Chao, Peng, Fabian, and Ojha, 2012); (5) Haiti (Aiken *et al.*, 2016); (6) San Jacinto fault, southern California (Chao, Peng, Fabian, and Ojha, 2012); (7) Queen Charlotte margin, Canada (Aiken *et al.*, 2013); (8) Sumbawa, Indonesia (Fuchs *et al.*, 2014; Bansal *et al.*, 2016); (9) Denali fault, Canada (Aiken *et al.*, 2015); (10) Ecuador (this study); (11) southwestern Ryukyu, Japan (Chao and Obara, 2016), (12), Kanto, Japan (Chao and Obara, 2016); (13) western Kyushu, Japan (Chao and Obara, 2016); (14) central Hikurangi Margin, New Zealand (Fry *et al.*, 2011; Chao *et al.*, 2013; Chao and Yu, 2018); (15) central Hokkaido, Japan (Chao and Obara, 2016), (16) southeastern Kyushu, Japan (Chao and Obara, 2016); (17) Guerrero, Mexico (Zigone *et al.*, 2012); (18) southern Taiwan (Chao, Peng, Wu, *et al.*, 2012); (19) eastern Shikoku, Japan (Chao and Obara, 2016); (20) Tokai, Japan (Chao and Obara, 2016); (21) southern Kii, Japan (Chao and Obara, 2016); (22) northern Kii, Japan (Chao and Obara, 2016); (23) western Shikoku, Japan (Chao and Obara, 2016); (24) Vancouver Island, Canada (Rubinstein *et al.*, 2009); (25) southern Chile (this study); and (26) Parkfield, central California (Peng *et al.*, 2009). The color version of this figure is available only in the electronic edition.

ac.jp/~idehara/wtd0/Welcome.html (last accessed August 2017) (Idehara *et al.*, 2014).

## ACKNOWLEDGMENTS

The authors thank the Servicio Geologico Colombiano (SGC) for providing the continuous access to data. The authors also thank two anonymous reviewers and Guest Editor Marino Protti, for their valuable comments. Kevin Chao is supported by the Northwestern Institute for Complex Systems (NICO) at Northwestern University through the Northwestern Data Science Scholars Fellowship. He is also supported by the Japan Society for the Promotion of Science (JSPS) through Awards P12329 and Grants-in-Aid for Scientific Research (KAKENHI) 23244091. Zhigang Peng is supported by National Science Foundation Grant Numbers EAR-0956051 and EAR-1543399.

## REFERENCES

Aiken, C., and Z. Peng (2014). Dynamic triggering of microearthquakes in three geothermal/volcanic regions of California, *J. Geophys. Res.* **119,** 6992–7009, doi: 10.1002/2014JB011218.

Aiken, C., K. Chao, H. Gonzalez-Huizar, R. Douilly, Z. Peng, A. Deschamps, E. Calais, and J. S. Haase (2016). Exploration of remote triggering: A survey of multiple fault structures in Haiti, *Earth Planet. Sci. Lett.* **455,** 14–24, doi: 10.1016/j.epsl.2016.09.023.

Aiken, C., Z. Peng, and K. Chao (2013). Tremors along the Queen Charlotte Margin triggered by large teleseismic earthquakes, *Geophys. Res. Lett.* **40,** 829–834, doi: 10.1002/grl.50220.

Aiken, C., J. P. Zimmerman, Z. Peng, and J. I. Walter (2015). Triggered seismic events along the eastern Denali fault in northwest Canada following the 2012 Mw 7.8 Haida Gwaii, 2013 Mw 7.5 Craig, and two Mw > 8.5 teleseismic earthquakes, *Bull. Seismol. Soc. Am.* **105,** 1165–1177, doi: 10.1785/0120140156.

Bansal, A. R., D. Yao, Z. Peng, and D. Sianipar (2016). Isolated regions of remote triggering in South/Southeast Asia following the 2012 Mw 8.6 Indian Ocean earthquake, *Geophys. Res. Lett.* **43,** 10,654–10,662, doi: 10.1002/2016GL069955.

Bartlow, N. M., D. A. Lockner, and N. M. Beeler (2012). Laboratory triggering of stick-slip events by oscillatory loading in the presence of pore fluid with implications for physics of tectonic tremor, *J. Geophys. Res.* **117,** no. B11, doi: 10.1029/2012JB009452.

Bedford, J., M. Moreno, and B. Schurr (2015). Investigating the final seismic swarm before the Iquique-Pisagua 2014 Mw 8.1 by comparison of continuous GPS and seismic foreshock data, *Geophys. Res. Lett.* **42,** 3820–3828, doi: 10.1002/2015GL063953.

Bernal-Olaya, R., P. Mann, and C. A. Vargas (2015). Earthquake, tomographic, seismic reflection, and gravity evidence for a shallowly dipping subduction zone beneath the Caribbean Margin of Northwestern Colombia in *Petroleum Geology and Potential of the Colombian Caribbean Margin*, C. Bartolini and P. Mann (Editors), AAPG Memoir, Vol. 108, 247–270.

Beroza, G. C., and S. Ide (2011). Slow earthquakes and nonvolcanic tremor, *Annu. Rev. Earth Planet. Sci.* **39,** 271–296, doi: 10.1146/annurev-earth-040809-152531.

Bezada, M. J., A. Levander, and B. Schmandt (2010). Subduction in the southern Caribbean: Images from finite-frequency P wave tomography, *J. Geophys. Res.* **115,** no. B12333, doi: 10.1029/2010JB007682.

Bockholt, B. M., C. A. Langston, H. R. DeShon, S. Horton, and M. Withers (2014). Mysterious tremor-like signals seen on the Reelfoot Fault, northern Tennessee, *Bull. Seismol. Soc. Am.* **104,** 2194–2205, doi: 10.1785/0120140030.

Chao, K., and K. Obara (2016). Triggered tectonic tremor in various types of fault systems of Japan following the 2012 $M_w$ 8.6 Sumatra earthquake, *J. Geophys. Res.* **121,** 170–187, doi: 10.1002/2015JB012566.

Chao, K., and C. Yu (2018). A MATLAB GUI for examining triggered tremor: A case study in New Zealand, *Seismol. Res. Lett.* doi: 10.1785/0220180057.

Chao, K., Z. Peng, A. Fabian, and L. Ojha (2012). Comparisons of triggered tremor in California, *Bull. Seismol. Soc. Am.* **102,** 900–908, doi: 10.1785/0120110151.

Chao, K., Z. Peng, H. Gonzalez-Huizar, C. Aiken, B. Enescu, H. Kao, A. A. Velasco, K. Obara, and T. Matsuzawa (2013). A global search for triggered tremor following the 2011 Mw 9.0 Tohoku earthquake, *Bull. Seismol. Soc. Am.* **103,** no. 2B, 1551–1571, doi: 10.1785/0120120171.

Chao, K., Z. Peng, Y.-J. Hsu, K. Obara, C. Wu, K.-E. Ching, S. van der Lee, H.-C. Pu, P.-L. Leu, and A. Wech (2017). Temporal variation of tectonic tremor activity in southern Taiwan around the 2010 ML6.4 Jiashian earthquake, *J. Geophys. Res.* **122,** 5417–5434, doi: 10.1002/2016JB013925.

Chao, K., Z. Peng, C. Wu, C.-C. Tang, and C.-H. Lin (2012). Remote triggering of non-volcanic tremor around Taiwan, *Geophys. J. Int.* **188,** 301–324, doi: 10.1111/j.1365-246X.2011.05261.x.

Chiarabba, C., P. De Gori, C. Faccenna, F. Speranza, D. Seccia, V. Dionicio, and G. A. Prieto (2016). Subduction system and flat slab beneath the Eastern Cordillera of Colombia, *Geochem., Geophys. Geosys.* **17,** 16–27, doi: 10.1002/2015GC006048.

Chicangana, G. (2005). The Romeral fault system: A shear and deformed extinct subduction zone between oceanic and continental lithospheres in northwestern South America, *Earth Sci. Res. J.* **9,** 51–66.

Dimate, C., L. Rivera, A. Taboada, B. Delouis, A. Osorio, E. Jimenez, A. Fuenzalida, A. Cisternas, and I. Gomez (2003). The 19 January 1995 Tauramena (Colombia) earthquake: Geometry and stress regime, *Tectonophysics* **363,** 159–180, doi: 10.1016/S0040-1951(02)00670-4.

Ego, F., M. Sebrier, and H. Yepes (1995). Is the Cauca-Patia and Romeral fault system left or right lateral?, *Geophys. Res. Lett.* **22,** 33–36.

Frank, W. B. (2016). Slow slip hidden in the noise: The intermittence of tectonic release, *Geophys. Res. Lett.* **43,** 10,125–10,133, doi: 10.1002/2016GL069537.

Frank, W. B., M. Radiguet, B. Rousset, N. M. Shapiro, A. L. Husker, V. Kostoglodov, N. Cotte, and M. Campillo (2015). Uncovering the geodetic signature of silent slip through repeating earthquakes, *Geophys. Res. Lett.* **42,** 2774–2779, doi: 10.1002/2015GL063685.

Frank, W. B., N. M. Shapiro, V. Kostoglodov, A. L. Husker, M. Campillo, J. S. Payero, and G. A. Prieto (2013). Low-frequency earthquakes in the Mexican Sweet Spot, *Geophys. Res. Lett.* **40,** 2661–2666, doi: 10.1002/grl.50561.

Fry, B., K. Chao, S. Bannister, Z. Peng, and L. Wallace (2011). Deep tremor in New Zealand triggered by the 2010 Mw8.8 Chile earthquake, *Geophys. Res. Lett.* doi: 10.1029/2011GL048319.

Fuchs, F., M. Lupi, and S. A. Miller (2014). Remotely triggered nonvolcanic tremor in Sumbawa, Indonesia, *Geophys. Res. Lett.* **41,** 4185–4193, doi: 10.1002/2014GL060312.

Gallego, A., R. M. Russo, D. Comte, V. Mocanu, R. E. Murdie, and J. C. VanDecar (2013). Tidal modulation of continuous nonvolcanic seismic tremor in the Chile triple junction region, *Geochem. Geophys. Geosys.* 1–13, doi: 10.1002/ggge.20091.

Gao, X., and K. Wang (2017). Rheological separation of the megathrust seismogenic zone and episodic tremor and slip, *Nature* **543,** 416–419, doi: 10.1038/nature21389.

Gomberg, J. (2010). Lessons from (triggered) tremor, *J. Geophys. Res.* **115,** no. B10302, doi: 10.1029/2009JB007011.

Gomberg, J., S. Prejean, and N. Ruppert (2012). Afterslip, tremor, and the Denali fault earthquake, *Bull. Seismol. Soc. Am.* **102,** 892–899, doi: 10.1785/0120110142.

Gonzalez-Huizar, H., A. A. Velasco, Z. Peng, and R. Castro (2012). Remote triggered seismicity caused by the 2011, M9.0 Tohoku, Japan earthquake, *Geophys. Res. Lett.* **39,** L10302, doi: 10.1029/2012GL051015.

Guilhem, A., Z. Peng, and R. M. Nadeau (2010). High-frequency identification of non-volcanic tremor triggered by regional earthquakes, *Geophys. Res. Lett.* **37,** doi: 10.1029/2010GL044660.

Helffrich, G., J. Wookey, and I. Bastow (2013). *The Seismic Analysis Code: A Primer and User's Guide*, Cambridge University Press, New York, New York, 102–106.

Hutchison, A. A., and A. Ghosh (2017). Ambient tectonic tremor in the San Jacinto fault, near the Anza Gap, detected by multiple mini seismic arrays, *Bull. Seismol. Soc. Am.* **107,** 1985–1993, doi: 10.1785/0120160385.

Ide, S. (2012). Variety and spatial heterogeneity of tectonic tremor worldwide, *J. Geophys. Res.* **117,** no. B03302, doi: 10.1029/2011JB008840.

Idehara, K., S. Yabe, and S. Ide (2014). Regional and global variations in the temporal clustering of tectonic tremor activity, *Earth Planets Space* **66,** no. 66, doi: 10.1186/1880-5981-66-66.

Inbal, A., T. Cristea-Platon, J. Ampuero, G. Hillers, D. Agnew, and S. E. Hough (2018). Sources of long-range anthropogenic noise in southern California and implications for tectonic tremor detection, *Bull. Seismol. Soc. Am.* **108,** 3511–3527, doi: 10.1785/0120180130.

Ito, Y., R. Hino, S. Suzuki, and Y. Kaneda (2015). Episodic tremor and slip near the Japan Trench prior to the 2011 Tohoku-Oki earthquake, *Geophys. Res. Lett.* **42,** no. 6, 1725–1731, doi: 10.1002/2014GL062986.

Kano, M., N. Aso, T. Matsuzawa, S. Ide, S. Annoura, R. Arai, S. Baba, M. Bostock, K. Chao, K. Heki, *et al.* (2018). Development of a slow earthquake database, *Seismol. Res. Lett.* **89,** 1566–1575, doi: 10.1785/0220180021.

Kato, A., and S. Nakagawa (2014). Multiple slow-slip events during a foreshock sequence of the 2014 Iquique, Chile Mw 8.1 earthquake, *Geophys. Res. Lett.* **41,** 5420–5427, doi: 10.1002/2014GL061138.

Kato, A., K. Obara, T. Igarashi, H. Tsuruoka, S. Nakagawa, and N. Hirata (2012). Propagation of slow slip leading up to the 2011 Mw 9.0 Tohoku-Oki earthquake, *Science* **335,** 705–708, doi: 10.1126/science.1215141.

La Rocca, M., K. C. Creager, D. Galluzzo, and S. Malone (2009). Cascadia tremor located near plate interface constrained by S minus P wave times, *Science* **323,** no. 5914, 620–623.

Maeda, T., and K. Obara (2009). Spatiotemporal distribution of seismic energy radiation from low-frequency tremor in western Shikoku, Japan, *J. Geophys. Res.* **114,** doi: 10.1029/2008JB006043.

Obara, K. (2002). Nonvolcanic deep tremor associated with subduction in southwest Japan, *Science* **296,** 1679–1681, doi: 10.1126/science.1070378.

Obara, K., and A. Kato (2016). Connecting slow earthquakes to huge earthquakes, *Science* **353,** 253–257.

Peng, Z., and J. Gomberg (2010). An integrated perspective of the continuum between earthquakes and slow-slip phenomena, *Nature Geosci.* **3,** 599–607, doi: 10.1038/ngeo940.

Peng, Z., B. Fry, K. Chao, D. Yao, X. Meng, and A. Jolly (2018). Remote triggering of microearthquakes and tremor in New Zealand following the 2016 M7.8 Kaikoura earthquake, *Bull. Seismol. Soc. Am.* **108,** 1784–1793.

Peng, Z., H. Gonzalez-Huizar, K. Chao, C. Aiken, B. Moreno, and G. Armstrong (2013). Tectonic tremor beneath Cuba triggered by the Mw8.8 Maule and Mw9.0 Tohoku-Oki earthquakes, *Bull. Seismol. Soc. Am.* **103,** no. 1, 595–600, doi: 10.1785/0120120253.

Peng, Z., J. E. Vidale, K. C. Creager, J. L. Rubinstein, J. Gomberg, and P. Bodin (2008). Strong tremor near Parkfield, CA, excited by the

2002 Denali Fault earthquake, *Geophys. Res. Lett.* **35,** doi: 10.1029/2008GL036080.
Peng, Z., J. E. Vidale, A. G. Wech, R. M. Nadeau, and K. C. Creager (2009). Remote triggering of tremor along the San Andreas fault in central California, *J. Geophys. Res.* **114,** doi: 10.1029/2008JB006049.
Pfohl, A., L. M. Warren, S. Sit, and M. Brudzinski (2015). Search for tectonic tremor on the Central North Anatolian fault, Turkey, *Bull. Seismol. Soc. Am.* **105,** no. 3, 1779, doi: 10.1785/0120140312.
Rolandone, F., J.-M. Nocquet, P. A. Mothes, P. Jarrin, M. Vallée, N. Cubas, S. Hernandez, M. Plain, S. Vaca, and Y. Font (2018). Areas prone to slow slip events impede earthquake rupture propagation and promote afterslip, *Sci. Adv.* **4,** eaao6596, doi: 10.1126/sciadv.aao6596.
Rousset, B., R. Bürgmann, and M. Campillo (2019). Slow slip events in the roots of the San Andreas fault, *Sci. Adv.* **5,** eaav3274, doi: 10.1126/sciadv.aav3274.
Rubinstein, J. L., J. Gomberg, J. E. Vidale, A. G. Wech, H. Kao, K. C. Creager, and G. Rogers (2009). Seismic wave triggering of nonvolcanic tremor, episodic tremor and slip, and earthquakes on Vancouver Island, *J. Geophys. Res.* **114,** doi: 10.1029/2008JB005875.
Rubinstein, J. L., J. E. Vidale, J. Gomberg, P. Bodin, K. C. Creager, and S. D. Malone (2007). Non-volcanic tremor driven by large transient shear stresses, *Nature* **448,** 579–582, doi: 10.1038/nature06017.
Ruiz, S., M. Metois, A. Fuenzalida, J. Ruiz, F. Leyton, R. Grandin, C. Vigny, R. Madariaga, and J. Campos (2014). Intense foreshocks and a slow slip event preceded the 2014 Iquique Mw 8.1 earthquake, *Science* **345,** 1165–1169, doi: 10.1126/science.1256074.
Saez, M., S. Ruiz, S. Ide, and H. Sugioka (2019). Shallow non-volcanic tremor activity and potential repeating earthquakes in the Chile triple joint: Seismic evidence of the subduction of the active Nazca-Antartic spreading Center, *Seismol. Res. Lett.* doi: 10.1785/0220180394.
Shearer, P. M. (1999). *Introduction to Seismology*, Cambridge University Press, Cambridge, New York.
Shelly, D. R., and J. L. Hardebeck (2010). Precise tremor source locations and amplitude variations along the lower-crustal central San Andreas fault, *Geophys. Res. Lett* **37,** L14301, doi: 10.1029/2010GL043672.
Shelly, D. R., Z. Peng, D. P. Hill, and C. Aiken (2011). Triggered creep as a possible mechanism for delayed dynamic triggering of tremor and earthquakes. *Nature Geosci.* **4,** 384–388, doi: 10.1038/ngeo1141.
Suzuki, T., and T. Yamashita (2009). Dynamic modeling of slow earthquakes based on thermoporoelastic effects and inelastic generation of pores. *J. Geophys. Res.* **114,** doi: 10.1029/2008JB006042.
Syracuse, E. M., M. Maceira, G. A. Prieto, H. Zhang, and C. J. Ammon (2016). Multiple plates subducting beneath Colombia, as illuminated by seismicity and velocity from the joint inversion of seismic and gravity data, *Earth Planet. Sci. Lett.* **444,** 139–149, doi: 10.1016/j.epsl.2016.03.050.
Todd, E. K., and S. Y. Schwartz (2016). Tectonic tremor along the northern Hikurangi Margin, New Zealand, between 2010 and 2015, *J. Geophys. Res.* **121,** no. 12, 8706–8719, doi: 10.1002/2016JB013480.
Todd, E. K., S. Y. Schwartz, K. Mochizuki, L. M. Wallace, A. F. Sheehan, S. C. Webb, C. A. Williams, J. Nakai, J. Yarce, B. Fry, *et al.* (2018). Earthquakes and tremor linked to seamount subduction during shallow slow slip at the Hikurangi Margin, New Zealand, *J. Geophys. Res.* **123,** no. 8, 6769–6783, doi: 10.1029/2018JB016136.
Uchida, N., T. Iinuma, R. M. Nadeau, R. Bürgmann, and R. Hino (2016). Periodic slow slip triggers megathrust zone earthquakes in northeastern Japan, *Science* **351,** 488–492, doi: 10.1126/science.aad3108.
Vallée, M., J.-M. Nocquet, J. Battaglia, Y. Font, M. Segovia, M. Régnier, P. Mothes, P. Jarrin, D. Cisneros, S. Vaca, *et al.* (2013). Intense interface seismicity triggered by a shallow slow slip event in the Central Ecuador subduction zone, *J. Geophys. Res.* **118,** 2965–2981, doi: 10.1002/jgrb.50216.
van der Elst, N. J., and E. E. Brodsky (2010). Connecting near-field and far-field earthquake triggering to dynamic strain, *J. Geophys. Res.* **115,** doi: 10.1029/2009JB006681.
Velasco, A., S. Hernandez, and T. Parsons (2008). Global ubiquity of dynamic earthquake triggering, *Nature Geosci.* **1,** 375–379, doi: 10.1038/ngeo204.
Wagner, L. S., J. S. Jaramillo, L. F. Ramírez-Hoyos, G. Monsalve, A. Cardona, and T. W. Becker (2017). Transient slab flattening beneath Colombia, *Geophys. Res. Lett.* **44,** 6616–6623, doi: 10.1002/2017GL073981.
Wech, A. G., and K. C. Creager (2008). Automated detection and location of Cascadia tremor, *Geophys. Res. Lett.* **35,** doi: 10.1029/2008GL035458.
Yang, H., and Z. Peng (2013). Lack of additional triggered tectonic tremor around the Simi Valley and the San Gabriel Mountain in southern California, *Bull. Seismol. Soc. Am.* **103,** 3372–3378, doi: 10.1785/0120130117.
Zigone, D., D. Rivet, M. Radiguet, M. Campillo, C. Voisin, N. Cotte, A. Walpersdorf, N. M. Shapiro, G. Cougoulat, P. Roux, *et al.* (2012). Triggering of tremors and slow slip event in Guerrero, Mexico, by the 2010 Mw 8.8 Maule, Chile, earthquake, *J. Geophys. Res.* **117,** doi: 10.1029/2012JB009160.

# APPENDIX

## LOCATION OF TRIGGERED TREMOR WITH A SINGLE STATION

For tremor recorded by a single station with three-component seismograms, we used the following two steps to estimate possible source locations. We first obtained the *S–P* travel-time difference (La Rocca *et al.*, 2009; Frank *et al.*, 2013) of triggered tremor occurring within triggered tremor bursts (Shelly *et al.*, 2011). Next, we calculated the hypocentral distance to the station and then projected the distance to potential faulting interfaces.

To measure the *S–P* travel-time difference, we computed the cross-correlation between the *S*- and *P* waves of all tremor bursts. Our major assumption is the *S*-wave energy of triggered tremor is strong in the lower frequency range of tremor (i.e., 3–5 Hz), and the *P*-wave energy of tremor shows up in the higher frequency range (i.e., higher than 15 Hz) (Fig. 5). We first applied a 3–5 Hz filter in two horizontal components for *S* waves and a 15–25 Hz filter (for a sampling rate of 100 Hz) or a 5 Hz high-pass filter (for a sampling rate of 20 Hz) in the vertical component for *P* waves. We then calculated the envelope function and smoothed it with a sliding 2 s window. Next, we cross-correlated the low-frequency band in the north (and east) component with the high-frequency band in the *Z* component (Fig. 5b,d,f). Finally, we obtained a stacked cross-gram from the two cross-correlation functions. The center peak of the cross-grams is used as the time difference between the *S*- and *P* waves of a triggered tremor burst ($\Delta T_{S-P}$), in which positive lag times indicate the vertical component is before the horizontal component. We then took the average $\Delta T_{S-P}$ for all triggered tremor bursts and used it as a proxy for the *S–P* travel-time difference (Ⓔ Fig. S2).

The $S$–$P$ travel-time difference can be expressed as $\Delta T_{S-P} = T_S - T_P = (\frac{1}{V_S} - \frac{1}{V_P}) \times \text{dist}_{\text{hypo}}$, in which $T_P$ and $T_S$ are $P$ and $S$ travel times, respectively, and $V_P$ and $V_S$ are $P$ and $S$ seismic velocities, respectively. Hence, we estimated the hypocentral distance ($\text{dist}_{\text{hypo}}$) to the observed station with equation $\text{dist}_{\text{hypo}} = \Delta T_{S-P} \times [(V_P \times V_S)/(V_P - V_S)] = \Delta T_{S-P} \times 8.71$, with a nominal $P$-wave (6.34 km/s) and $S$-wave (3.67 km/s) velocity in the crust (Shearer, 1999). We also had to take into account the tremor depth, which depends on the tectonic environment, and the tectonic age for the subduction zone tremor. Here, we simply used a 20 km depth for inland fault tremor (strike slip or thrust fault) (Shelly and Hardebeck, 2010; Chao and Obara, 2016) and a 35-km depth for subduction zone tremor (Maeda and Obara, 2009). Finally, by combining the distance from the tremor hypocenter, we estimated the probable location of triggered tremor using data recorded by a single station.

To test the reliability of our single-station method, we applied our approach to locate triggered tremor in western Shikoku in southwestern Japan during the passing surface waves of the 11 April 2012 Sumatra earthquake (Chao and Obara, 2016). We compared triggered tremor burst locations from the multiple station method (red circles in Fig. 5c) with the single-station approach (open circles in Fig. 5c). We found the single-station method performed better at a greater epicentral distance (i.e., greater than 30 km). For stations closer to the source (e.g., station KWBH), the $S$–$P$ time exhibited larger fluctuations, resulting in larger differences (Fig. 5c).

We note the $P$-wave signals of low-frequency earthquakes within triggered tremor sources normally have a low signal-to-noise ratio (SNR). Hence, this single-station approach is valid only while the data are recorded by a high-quality seismic network such as the borehole stations of Hi-net. Nevertheless, with the observed $P$- and $S$-wave travel-time difference, we were able to obtain a rough estimate of the tremor source location (Fuchs *et al.*, 2014).

*Kevin Chao*[1]
*Department of Earth and Planetary Sciences*
*Northwestern University*
*2145 Sheridan Road, Room F374*
*Evanston, Illinois 60208 U.S.A.*
**kchao@northwestern.edu**

*Zhigang Peng*
*School of Earth and Atmospheric Sciences*
*Georgia Institute of Technology*
*311 Ferst Drive*
*Atlanta, Georgia 30332 U.S.A.*

*William B. Frank*
*Department of Earth Sciences*
*University of Southern California*
*3651 Trousdale Parkway, ZHS 103*
*Los Angeles, California 90089 U.S.A.*

*Germán A. Prieto*
*Departamento de Geociencias*
*Universidad Nacional de Colombia*
*Cra 30 #45 – 03*
*Bogotá, Colombia*

*Kazushige Obara*
*Earthquake Research Institute*
*University of Tokyo*
*1-1-1 Yayoi, Bunkyo-ku*
*Tokyo 113-0032, Japan*

Published Online 31 July 2019

[1] Also at Northwestern Institute on Complex Systems, Northwestern University, Evanston, Illinois 60208 U.S.A.